Metastable Helium: A New Determination of the Longest Atomic Excited-State Lifetime

S. S. Hodgman,[1] R. G. Dall,[1] L. J. Byron,[1] K. G. H. Baldwin,[1,*] S. J. Buckman,[2] and A. G. Truscott[1]

[1]*ARC Centre of Excellence for Quantum-Atom Optics, The Australian National University, Canberra, ACT 0200, Australia*
[2]*Research School of Physics and Engineering, The Australian National University, Canberra, ACT 0200, Australia*

Exited atoms may relax to the ground state by radiative decay, a process which is usually very fast (of order nanoseconds). However, quantum-mechanical selection rules can prevent such rapid decay, in which case these "metastable" states can have lifetimes of order seconds or longer. In this Letter, we determine experimentally the lifetime of the longest-lived neutral atomic state—the first excited state of helium (the $2\,^3S_1$ metastable state)—to the highest accuracy yet measured. We use laser cooling and magnetic trapping to isolate a cloud of metastable helium (He*) atoms from their surrounding environment, and measure the decay rate to the ground $1\,^1S_0$ state via extreme ultraviolet (XUV) photon emission. This is the first measurement using a virtually unperturbed ensemble of isolated helium atoms, and yields a value of 7870(510) seconds, in excellent agreement with the predictions of quantum electrodynamic theory.

Quantum electrodynamics (QED) is one of the most rigorously tested theories of modern physics, and helium—the simplest multi-electron atom—is a favored test bed for QED predictions of atomic structure [1]. While measurement of atomic energy levels has been performed with great precision matching that of theoretical QED determinations, measuring the lifetime of these levels is much less precise (often at the percent level), and usually has greater uncertainty than corresponding theory. Precise knowledge of these state lifetimes is another important test of QED, which enters into the calculation of transition decay rates, e.g., through the inclusion of higher order diagrammatic contributions to the perturbation expansion of the atom-light field Hamiltonian.

Knowledge of the He $2\,^3S_1$ state lifetime is important not just as a test of QED, but also because of the key role that He* plays in many environments. In addition to being the longest-lived neutral atomic state, the $2\,^3S_1$ level is the most energetic metastable state of any atomic species— some 20 eV above the ground state. Consequently, He* is an important source of stored energy in ionospheric and discharge plasmas where the large electron scattering cross section of He* also plays an important role [2]. Furthermore, the large stored energy not only allows efficient detection of He* atoms using charged particle techniques, but the long lifetime means that the $2\,^3S_1$ level acts as an effective ground state for laser cooling via the efficient 1083 nm transition to the $2\,^3P_2$ level. This makes He* a useful species for atom optics experiments where detection of individual particles is important [3].

The extremely long metastable lifetime arises from the fact that direct photon decay of the $2\,^3S_1$ state to the $1\,^1S_0$ ground state is doubly forbidden by quantum-mechanical selection rules. First, the metastable state shares the same angular momentum quantum number (S, $l = 0$) as the ground state (Fig. 1), which forbids decay via a single-

photon electric dipole transition. Second, the two electrons in the metastable state have parallel spins, while the ground state is a spin antiparallel configuration, requiring a low probability spin flip for the decay process. As a consequence, the most rapid decay process from the metastable to the ground state is via a magnetic-dipole-allowed, single-photon transition at 62.6 nm in the XUV region.
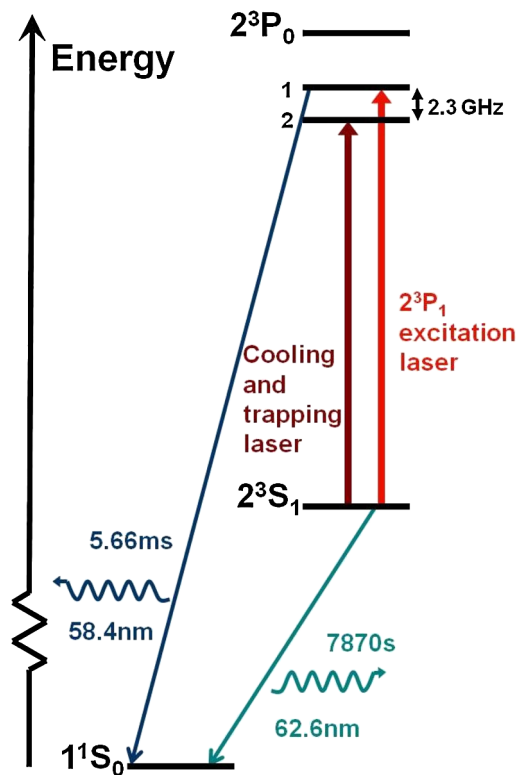

FIG. 1 (color online). Energy level diagram for helium. Excited-state decays to the ground state are indicated, along with laser transitions from the metastable $2\,^3S_1$ state.

The result of this doubly forbidden decay process is the longest excited state lifetime of any neutral atomic (cf. ionic [4,5]) species. Theoretical predictions of the magnetic dipole decay rate for the $2\,^3S_1$ state date back to the early calculations using QED theory by Drake [6], Feinberg and Sucher [7], and Johnson and Lin [8], who predicted values of 7870, 8330, and 7980 s, respectively, for the metastable lifetime. The historical progression of both experimental and theoretical values for the $2\,^3S_1$ lifetime are shown in Fig. 2. Later calculations by Johnson et al. [1] via an alternative QED approach using relativistic many-body perturbation theory yielded a similar result (7900 s). More recently, Lach and Pachucki [9] provided the most complete QED lifetime determination of 7860 s.

Note that while the numerical uncertainty associated with these calculations is often relatively small (three significant figures in Ref. [9]), the systematic uncertainty can be significantly greater and arises from incomplete estimates of the contribution of higher order terms omitted in the calculations. Consequently, the spread in the predicted values arising from the different approaches provides an indication of the theoretical uncertainty.

The only previous experimental estimate of the $2\,^3S_1$ lifetime dates back more than 30 years to the early measurements by Moos and Woodworth [10,11]. These experiments were conducted in an unstable and highly perturbed plasma discharge (the only effective source for exciting He* atoms through electron collision) which presents a challenging environment for the determination of the experimental parameters. Furthermore, the He* atoms were not isolated, which means that the effective lifetime of the $2\,^3S_1$ state can potentially be reduced by collisional deexcitation. Their initial estimate of ~4000 s with a factor of 3 uncertainty [10] was later refined to ~9000 s with a 30% uncertainty estimate [11]. Their technique not only needed an absolute measurement of the total 62.6 nm photon flux
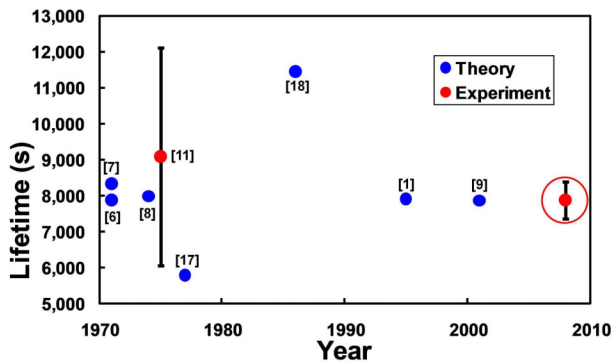
(requiring accurate calibration of the detection system), but also a precise knowledge of the He* atom number to determine the $2\,^3S_1$ state lifetime from the ratio of these two quantities, both of which are the source of considerable systematic and statistical uncertainty.

Our experiment improves upon this approach in two key areas. First, we obviate the need to measure the absolute number of He* atoms by measuring the $2\,^3S_1$ XUV photon emission rate to the ground state relative to the much higher (~10^6 times) $2\,^3P_1$ photon emission rate to the ground state (Fig. 1), which we have measured recently for the first time [12]. We therefore do not need to measure the (very long) $2\,^3S_1$ state decay time directly, and consequently are less influenced by perturbing collisions which can affect such measurements.

Second, we virtually eliminate such perturbations by isolating the He* atoms in a vacuum (Fig. 3). Like the earlier measurements, we initially generate He* atoms in a discharge source [13], but we then load these atoms via laser collimation, Zeeman slowing, and magneto-optic trapping techniques into the virtually unperturbed environment of a magnetic trap in an ultrahigh vacuum chamber. As recognized some years ago by Metcalf [14], the isolation provided by laser cooling and trapping potentially enables a significant improvement in both the systematic and statistical uncertainties in determining the $2\,^3S_1$ state lifetime.
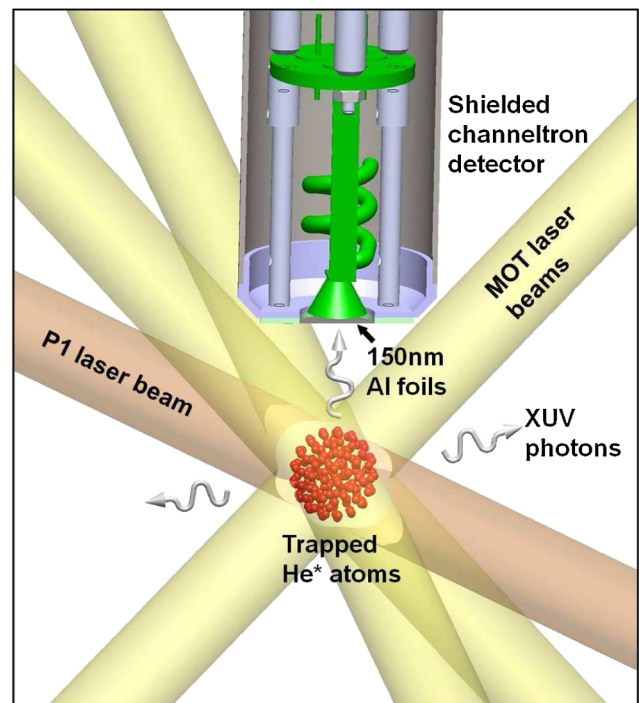

FIG. 2 (color online). Metastable state lifetimes. Theoretical and experimental determinations of the helium $2\,^3S_1$ lifetime with corresponding references (present result circled, only experimental error bars presented). References [17,18] deviate markedly from other theoretical predictions as they do not account adequately for electron correlations [1].

FIG. 3 (color online). Experimental schematic. The geometry of the 1083 nm MOT laser beams and the $2\,^3P_1$ excitation ($P1$) laser beams is shown relative to the detection system, comprising the channeltron with aluminium filters and shield (quadrupole magnetic field trapping coils not shown).

We load approximately 10^8 He* atoms into the magnetic quadrupole trap at temperatures of around 200 μK. The emitted XUV photons are counted using a channeltron detector, which can detect both the 62.6 nm XUV photons emitted by the $2\,^3S_1$ state and the 58.4 nm photons emitted by the $2\,^3P_1$ state. To ensure no stray He* atoms, ions, or photons are detected, the channeltron is enclosed in aluminium shielding. Two $\sim$150 nm thick aluminium foils covering the channeltron entrance allow the transmission of XUV photons with wavelengths <80 nm, but block longer wavelengths. The two foils are necessary in case there are pinholes and keep the background count rate to <0.02 Hz.

The experimental cycle commences by switching off the MOT and loading the atoms into the magnetic quadrupole trap. One hundred and fifty ms after the MOT laser has been switched off, we measure (for $\sim$0.5 s) the 62.6 nm XUV photon flux emitted from the ensemble of He* atoms confined in the magnetic trap. Because of the low photon flux from the $2\,^3S_1$ state, the counts are binned to increase the signal-to-noise ratio, and the bins averaged over 56 000 experimental cycles. The measured 62.6 nm photon count rate is shown in the main section of Fig. 4.

During the measurement period, the trap population decreases slightly due to infrequent collisions with background gas atoms. [Note that this decrease is not due to radiative decay of the metastable state which occurs over much longer ($\sim$8000 s) timescales.] A fitted exponential is
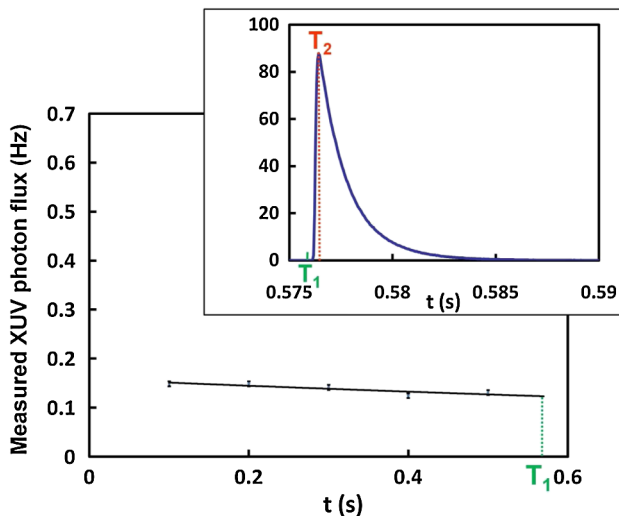

FIG. 4 (color online). XUV photon flux averaged over 56 000 experimental cycles. Main figure: count rate for 62.6 nm photons emitted by magnetically trapped $2\,^3S_1$ atoms. Error bars are associated with statistical (1σ) fluctuations in the photon count rate. The fitted exponential is used to derive the integrated flux at point T_1. Inset: count rate for 58.4 nm photons emitted by untrapped $2\,^3P_1$ atoms. The 1083 nm illumination saturates the excited-state population at point T_2. Note the change in the time scale and count rates for the inset.

then used to normalize the data to yield a $2\,^3S_1$ photon count rate at constant atom number at time T_1.

Immediately after T_1, the trap is switched off and a retro-reflected 1083 nm laser beam illuminates the untrapped cloud to saturate the $2\,^3S_1$–$2\,^3P_1$ transition. This results in a sharp increase in the measured XUV photon flux (inset to Fig. 4) due to the much faster 58.4 nm photon decay from $2\,^3P_1$ to the ground state [effective decay lifetime $\sim$5.66(25) ms] [12]. The higher flux allows a much shorter binning time, making the count rate appear continuous. During the untrapped phase, there is negligible expansion of the cloud, and consequently, the number of emitting atoms for which the flux is measured is unchanged.

The $2\,^3P_1$ photon count rate at the saturation point (T_2) is then measured, and the ratio of this rate to the $2\,^3S_1$ rate at T_1 is then used to determine the $2\,^3S_1$ lifetime. The degree of saturation was determined using the technique developed by DePue *et al.* [15] as used in our previous experiments [12,16]. Note that the trap loss due to background collisions is negligible during the short time that elapses between T_1 and T_2. A complete experimental cycle (including trap loading) lasts for $\sim$3 s.

During the second phase of the measurement cycle, saturation of the $2\,^3S_1$–$2\,^3P_1$ transition places 50% of the ensemble in the $2\,^3P_1$ state. The ratio of the $2\,^3P_1$ XUV photon flux to the $2\,^3S_1$ XUV photon flux, combined with the known $2\,^3P_1$–$1\,^1S_0$ decay rate [12] and the 50% excited state population fraction, directly yields the $2\,^3S_1$ lifetime. The value of 7870(510) s (1σ uncertainty 6.5%) is in excellent agreement with the most complete theoretical determinations presented in Fig. 2.

In addition to the statistical uncertainty in the data from Fig. 4 (1.7%), we include a number of independent contributions to the error budget (Table I). First, we correct our measured lifetime by allowing for the relative detection efficiency at 58.4 and 62.6 nm arising from the wavelength dependence of the transmission of the filters and of the channeltron quantum efficiency. There is an associated measurement error with this correction (since the manufacturers specifications have a finite accuracy) which has an overall contribution to the error budget of 3.1%.

Second, we measure the degree of (almost complete) saturation of the $2\,^3S_1$–$2\,^3P_1$ transition, which we deter-

TABLE I. Error budget for the $2\,^3S_1$ lifetime.

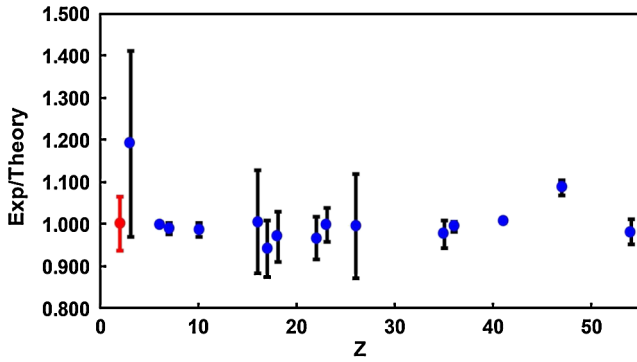| Source	Uncertainty (%)
Decay rate ratio (statistical)	1.7
Relative detection efficiency correction	3.1
Population saturation	2.3
Channeltron linearity	<1
Emission anisotropy	<1
Finite binning time	2.1
$2\,^3P_1$ lifetime	4.4
Combined uncertainty	6.5

FIG. 5 (color online). Helium isoelectronic sequence. The ratio of the experimental to the most recent theoretical $2\,^3S_1$ lifetime, along with experimental uncertainties, for the helium-like isoelectronic sequence. Figure adapted from Ref. [1], with He ($Z = 2$) = present experimental value divided by the theoretical value from Ref. [9].

mine to within an uncertainty of 2.3%. This represents the statistical error in correcting the population value (which can only reach 50% at infinite saturation laser power) by fitting the fluorescence saturation curve as a function of laser power.

Third, we determine the linearity of the channeltron detector by measuring the ratio of the $2\,^3P_1$–$1\,^1S_0$ XUV count rate on the channeltron to the $2\,^3P_1$–$2\,^3S_1$ infrared (1083 nm) emission as detected by a photodiode. The ratio is consistent with a statistical fitting uncertainty of less than 1%.

Fourth, the $2\,^3S_1$ atoms confined in the trap on average experience an isotropic magnetic field over the volume of the trap and consequently radiate isotropically on average. Emission from the $2\,^3P_1$–$2\,^3S_1$ state occurs when the atoms are untrapped. To ensure that stray laboratory magnetic fields do not systematically affect the spatial distribution of the $2\,^3P_1$ emission, we observe the resulting 58.4 nm XUV photon flux in the presence of weak (several Gauss) imposed magnetic fields. The detected 58.4 nm photon signal was unchanged for all the magnetic field strengths investigated, within the statistical noise of the measurements. The anisotropy tests yield an uncertainty contribution of less than 1%.

Finally, there is a contribution due to the use of finite time bins in the $2\,^3S_1$ XUV flux fitting process, which we estimate at 2.1%. This comprises a variation in the correction for the 62.6 nm flux decay due to the finite width and position of the time bins which is partially statistical in nature due to the measurement uncertainty in the data points.

Apart from the population saturation and the finite time binning, the uncertainties have a statistical or pseudorandom character. The systematic correction for the population saturation itself has a significant statistical uncertainty component, as does the variation due to finite time binning.

We have therefore combined these uncertainties quadratically with the uncertainty in the previously [12] measured $2\,^3P_1$–$1\,^1S_0$ decay rate (4.4%), to yield a total error budget of 6.5%.

Furthermore, the experiment determines the ratio of the $2\,^3S_1{:}2\,^3P_1$ decay times to even greater precision (better than 5%). If the most recent theoretical value for the $2\,^3P_1$–$1\,^1S_0$ decay time is assumed to be correct (5.63 ms [9]), then the measured $2\,^3S_1{:}2\,^3P_1$ decay time ratio yields a $2\,^3S_1$ lifetime of 7850(370) s.

The result of our He* experimental measurement can be placed in the context of the two-electron QED testbed for ionized species as shown in the heliumlike isoelectronic sequence of Fig. 5. Our measurement anchors the isoelectronic sequence at low Z which, until these experiments, was a region of considerable uncertainty. This greatly improved determination of the helium $2\,^3S_1$ lifetime provides further validation for quantum electrodynamic theory.

*kenneth.baldwin@anu.edu.au
[1] W. R. Johnson, D. R. Plante, and J. Sapirstein, Adv. At. Mol. Opt. Phys. **35**, 255 (1995).
[2] L. J. Uhlmann, R. G. Dall, A. G. Truscott, M. D. Hoogerland, K. G. H. Baldwin, and S. J. Buckman, Phys. Rev. Lett. **94**, 173201 (2005).
[3] K. G. H. Baldwin, Contemp. Phys. **46**, 105 (2005).
[4] M. Roberts, P. Taylor, G. P. Barwood, P. Gill, H. A. Klein, and W. R. C. Rowley, Phys. Rev. Lett. **78**, 1876 (1997).
[5] M. Roberts, P. Taylor, G. P. Barwood, W. R. C. Rowley, and P. Gill, Phys. Rev. A **62**, 020501(R) (2000).
[6] G. W. F. Drake, Phys. Rev. A **3**, 908 (1971).
[7] G. Feinberg and J. Sucher, Phys. Rev. Lett. **26**, 681 (1971).
[8] W. R. Johnson and C.-p. Lin, Phys. Rev. A **9**, 1486 (1974).
[9] G. Lach and K. Pachucki, Phys. Rev. A **64**, 042510 (2001).
[10] J. R. Woodworth and H. W. Moos, Phys. Rev. Lett. **30**, 775 (1973).
[11] H. W. Moos and J. R. Woodworth, Phys. Rev. A **12**, 2455 (1975).
[12] R. G. Dall, K. G. H. Baldwin, L. J. Byron, and A. G. Truscott, Phys. Rev. Lett. **100**, 023001 (2008).
[13] J. A. Swansson, K. G. H. Baldwin, M. D. Hoogerland, A. G. Truscott, and S. J. Buckman, Appl. Phys. B **79**, 485 (2004).
[14] H. Metcalf, J. Opt. Soc. Am. B **6**, 2206 (1989).
[15] M. T. DePue, S. L. Winoto, D. J. Han, and D. S. Weiss, Opt. Commun. **180**, 73 (2000).
[16] R. G. Dall and A. G. Truscott, Opt. Commun. **270**, 255 (2007).
[17] C. D. Lin, W. R. Johnson, and A. Dalgarno, Phys. Rev. A **15**, 154 (1977).
[18] J. Krause, Phys. Rev. A **34**, 3692 (1986).